THE ASTROPHYSICAL JOURNAL, 407:556–563, 1993 April 20

BBXRT AND *GINGA* OBSERVATIONS OF THE SEYFERT 1 GALAXY MARKARIAN 335

T. J. TURNER,[1,3] K. NANDRA,[2,4] A. A. ZDZIARSKI,[1,6] K. JAHODA,[1] G. M. MADEJSKI,[1,3]
F. MARSHALL,[1] R. F. MUSHOTZKY,[1] R. PETRE,[1] K. A. POUNDS,[2] A. P. SMALE,[1,3]
P. SERLEMITSOS,[1] AND K. WEAVER[1,5]
Received 1992 June 25; accepted 1992 October 28

ABSTRACT

We present new X-ray observations of Mrk 335 in the 0.4–10 keV band using BBXRT and in the 2–20 keV band with *Ginga*. The BBXRT data show a break to a softer spectrum below ~1 keV. The *Ginga* data show evidence for variability in absorption, uncorrelated with flux changes of the continuum source. The inconsistency between the opacity observed at the iron K edge and at softer X-ray energies implies that the absorber has an ionization state ~FeXV. We suggest that the nuclear emission can be explained by a self-consistent pair cascade model as developed by Zdziarski et al. and Zdziarski and Coppi, where the compactness parameter inferred from the spectral fits to both data sets is in good agreement with the value calculated from the ratio of observed X-ray luminosity and variability time scale.

Subject headings: galaxies: individual (Markarian 335) — galaxies: Seyfert — X-rays: galaxies

1. INTRODUCTION

The Seyfert 1 galaxy Mrk 335 ($z = 0.026$; R.A. (1950) = $00^h03^m45^s.0$, Decl. (1950) = 19°55′30″) was first detected in X-rays by *UHURU* (Tananbaum et al. 1978). It was observed with the *Einstein* Observatory (Halpern 1982), where it exhibited a soft X-ray flare lasting ~10 ks (Lee et al. 1988). Subsequent *EXOSAT* observations by Pounds et al. (1987) (see also Turner & Pounds 1988, hereafter TP88, and Turner & Pounds 1989) established the existence of a two-component X-ray spectrum in the 0.1–10 keV band, including a steep spectral component dominating the soft X-ray spectrum. Neither the form of this soft component nor the break energy between the two components could be well determined, as the *EXOSAT* LE detector/filter combination had very poor energy resolution. *EXOSAT* also observed rapid variability in the soft excess component, with a factor of ~2 increase in 10 hr during the long observation. Soft X-ray excess components have been hypothesized to originate in the inner regions of an accretion disk. In this support of that idea, other waveband data have suggested that an accretion disk does exist in Mrk 335. *IUE* observations have shown Mrk 335 to turn up in the ultraviolet, having an excess continuum component near 3000 Å (Malkan & Sargent 1982). In addition, Van Groningen (1987) suggested an accretion disk to explain the asymmetric optical line profiles observed in this object. Pounds et al. (1987) go on to suggest that the observed strong UV component and the X-ray soft excess could be two ends of a (mainly unobservable) XUV spectral feature, which they modeled as an accretion disk radiating locally as a self-consistent atmosphere. While the hard and soft X-ray components appeared uncorrelated on short (less than 1 day) time scales, six *EXOSAT* observations spread over a 2 yr period suggested that the two spectral components track each other over the large amplitude changes in source flux (up to a factor of ~7) which occur on time scales of years (TP88).

2. THE OBSERVATIONS

2.1. *The BBXRT Data*

The Broad-Band X-Ray Telescope (BBXRT) was flown with the ASTRO ultraviolet instruments as part of the *Columbia* (STS-35) shuttle payload on a 9 day mission between 1990 December 2–10. The BBXRT instrument was designed and built at Goddard Space Flight Center and is described in detail in Serlemitsos et al. (1992). The instrument consisted of two co-aligned X-ray telescopes, with mirrors made of thin, nested, gold coated aluminum foils. These mirrors were among the first allowing reflection of X-ray photons above ~4 keV, focusing X-rays onto cooled segmented lithium-drifted silicon solid state spectrometers. The effective bandpass of this combination was ~0.3–12 keV. Each of the telescopes had a detector consisting of 5 pixels, with the central pixel having a 4′ diameter field of view, and the total diameter of 17′. The effective area of each telescope was 160 cm^2 at 1.5 keV and 75 cm^2 at 7 keV, with energy resolution of ~0.02 counts s^{-1} in the central pixel, and 0.1 counts s^{-1} in each outer pixel. We note here that the calibration for the BBXRT instrument has improved since the publication of the preliminary results in Turner et al. (1992), specifically with regard to the data screening and background subtraction, and thus this paper should be considered the definitive result for the BBXRT observation of Mrk 335.

The observation of Mrk 335 began on day 339 of 1990, with a start time of 20:30 (UT) and an exposure of 2160 s. Although the observation began during orbit day, after 600 s the shuttle was in orbit night. The observation was ended when the Earth angle fell below 90°. The effective exposure time of aceptable data was thus 1560 s. The observation was free of the South Atlantic Anomaly, and the data were free of contamination by Solar X-rays (Sun angle ~114°). Thus, most of the Mrk 335 observation was made during a period of minimum X-ray background.

Although there is no aspect solution available for this observation, the two axis pointing system gimbal data allowed a determination of pointing position to within ~10′. As there is

[1] Laboratory for High Energy Astrophysics, NASA/Goddard Space Flight Center, Greenbelt, MD 20771.
[2] Department of Physics, Leicester University, Leicester, England.
[3] Universities Space Research Association.
[4] Institute of Astronomy, Cambridge University, Cambridge, England.
[5] Department of Astronomy, University of Maryland, College Park, MD 20642.
[6] N. Copernicus Astronomical Center, Warsaw, Poland.

no other X-ray source known within 10′ (confirmed by examination of the 25 ksec *ROSAT* PSPC image recently received by the authors), we can confirm this observation to be of the Seyfert 1 galaxy Mrk 335.

In this observation, source counts were observed in detectors A0, A2, B0, and B4. As the source counts are approximately equal in B0 and B4, we deduce that the source lies under the B strut. Since the use of the B0, B4, and A2 data does not significantly improve the signal-to-noise ratio we use only A0 data. Since the source counts in A0 are much greater than in A2, we conclude that the source lies approximately 2′ offset from the center of A0. The response matrix used for spectral fitting includes a correction for such an offset, and the data are binned to contain a minimum of 20 counts per channel, so that a χ^2 spectral fitting algorithm can be applied.

There were two components to the background in the data: the internal part, and the sky background. As the most difficult background subtraction problem in BBXRT data is the elimination of the strong geocoronal lines from the bright Earth, and as this analysis is sensitive to the exact spectrum at soft X-ray energies, we used only the nighttime data (1560 s out of 2160 s data set) for spectral fitting.

The internal background rate for any particular observation is related to the guard A rate (see Weaver et al. 1993). For this observation, the mean guard rate was determined to be 1700 counts per 8 s bin. The sky background contribution was determined using a series of background observations made with the same orbital constraints as our observation (Weaver et al. 1993). As the night sky background file was made up from a large number of nighttime sky pointings, this means that a mean diffuse sky background was subtracted as well. This approximation is considered acceptable as the diffuse background yielded a count rate of less than 5% of the count rate of Mrk 335 in the BBXRT data. To confirm the validity of this approximation, the diffuse X-ray background component was varied by $\pm 50\%$, this was found to result in a difference in derived spectral index of $\Delta\alpha = 0.07$, less than the 1 σ error derived for that parameter.

2.2. *The Ginga Data*

Here we present two *Ginga* observations of Mrk 335 taken in 1987 and 1988. The observation log is shown in Table 1. Standard background subtraction techniques have been applied (see Hayashida et al. 1989 for details), using multiple sky pointings to model the background level and spectrum during the time of the source observation. The diffuse X-ray background uncertainty was estimated by again undertaking spectral fitting with an appropriate portion of the diffuse background spectrum added to and subtracted from the source spectrum, and then the derived systematic error was added in quadrature to the statistical errors already included in the data. The *Ginga* spectra described here include only the top-layer data (to maximize the signal-to-noise ratio below 10 keV) and are restricted to the 2–10 keV range (to avoid contamination by silver fluorescence K line at 22–25 keV from the collimator coating).

3. SPECTRAL MODELING

In this section, we present the results of spectral modeling of the data from both instruments. We use a commonly adopted parameterization of the spectra as power laws modified by absorption in the line of sight, both due to the interstellar medium of our galaxy as well as matter intrinsic to Mrk 335. However, such an ad hoc parameterization, while generally providing a satisfactory fit to X-ray AGN data, does not strongly constrain intrinsic emission mechanisms. In § 5, we show that a self-consistent physical model, incorporating electron-positron pairs interacting with the soft UV radiation from the putative accretion disk, fits the data well.

3.1. *The BBXRT Data*

The BBXRT data were tested against several spectral models. The first model, a simple power law plus absorption by cold, cosmic abundance material (Morrison & McCammon 1983) gave an acceptable fit. The parameters are shown in Table 2 with their associated 90% confidence limits (Lampton, Margon, & Bowyer 1976). The fit to the entire BBXRT data set, covering 0.4–10 keV, yielded an energy index of 1.19 ± 0.14 and zero absorption (less than 2.4×10^{20} cm^{-2}). As the best-fit absorption was less than the Galactic value we fixed absorption at Galactic, 4×10^{20} cm^{-2} (derived from 21 cm data; Stark et al. 1992), and refitted (Table 2). We now obtain an energy index of 1.35 ± 0.15. Both of these fits are statistically acceptable. Fitting the data in a softer bandpass, 0.4–1.0 keV, with fixed Galactic absorption as before, we obtain an energy index of 2.03 ± 0.40. The fits indicate a significant spectral steepening towards softer X-ray energies. Since the *EXOSAT* data clearly indicate an excess of soft ($\lesssim 1$ keV) X-rays over the extrapolated greater than 1 keV continuum, a more complex model is warranted. To establish the spectral shape of the continuum above 2 keV, we fitted the 2–10 keV BBXRT data for comparison and obtained an energy index of 0.87 ± 0.32 (Table 2) with a 2–10 keV flux of $\sim 8.4 \pm 0.5 \times 10^{-12}$ ergs cm^{-2} s^{-1}.

TABLE 1

OBSERVING LOG FOR MARKARIAN 335

Instrument	Year/day (UT)	Exposure (10^3 s)	Count Rate	2–10 keV Flux ($\times 10^{-11}$ ergs cm^{-2} s^{-1})
UHURU	1971/1972[a]	[a]	1.2 ± 0.42[a]	2.04 ± 0.3[a]
HEAO 1/A2	1978/188	5638	0.8 ± 0.15	1.1 ± 0.2
Einstein HRI	1981/01	15.0	0.51	1.46 ± 0.1
Einstein MPC	1981/01	29.4	0.50	1.46 ± 0.1
EXOSAT LT + ME	1983–1984	...	...	$0.3 \rightarrow 1.9$
Ginga	1987/337	17.5	4.1 ± 0.1	0.91 ± 0.16
Ginga	1988/329	19.8	9.5 ± 0.1	2.00 ± 0.16
BBXRT	1990/339	1.56	(A0)0.5 ± 0.1	0.84 ± 0.05

[a] From scanning observations, using point summation technique (Tananbaum et al. 1978). Flux and count rate quoted are over the 2–6 keV band.

TABLE 2

FITS TO THE BBXRT DATA

Model	Energy Range (keV)	A_{pl} ($\times 10^{-3}$)	α	A_2 ($\times 10^{-3}$)	α_2 or T (keV)	N_H (10^{21} cm^{-2})	χ_r^2/d.o.f.
PL + absorption	0.4–10	1.87	1.19 ± 0.14			$0.0 < 0.24$	0.86/30
PL + absorption	0.4–10	2.12	1.35 ± 0.15			0.4(f)	1.13/31
PL + absorption	2–10	1.46	0.87 ± 0.32			0.4(f)	1.08/13
PL + BB + absorption	0.4–10	1.52	0.87(f)	0.071	0.10 ± 0.03	0.4(f)	0.74/30
2 PL + absorption	0.4–10	1.46	0.87(f)	0.55	$2.95^{+1.05}_{-0.85}$	0.4(f)	0.64/30

NOTES.—"f" denotes a fixed parameter. Error ranges are 90% confidence for one parameter of interest ($\chi^2 + 2.7$). A_{pl} and A_2 are the hard power law and soft component normalizations, respectively, at 1 keV in photons cm^{-2} s^{-1}.

Extrapolating the 2–10 keV power-law fit (again, absorbed by our galaxy) down to 0.4 keV, we see that the soft X-ray data lie systematically above the model below about 1.0 keV (Fig. 1). Fitting a two-power-law model reduced the value of χ^2 by 14 (Table 2), giving an F statistic of 11 (indicating an improvement in the fit at more than 95% confidence) and a soft component energy index of 2.95 (Table 2). Alternatively we can model the soft spectrum as a blackbody of temperature 0.10 ± 0.03 keV, giving an F statistic of 8 (90% confidence). As the *EXOSAT* data already excluded partial covering by cold material or leakage of hard component flux through an ionized absorber as the *sole* origin for the soft excess, we do not present such a parameterization of the BBXRT data. Fitting separate absorption for each spectral component produces no significant (at more than 90% confidence) improvement to any of the two-component fits.

How constant is the ratio of the hard-to-soft components? Fitting, for comparison, the best-fit indices derived from the *EXOSAT* data ($\alpha_{hard} = 0.69$, $\alpha_{soft} = 2.65$, and Galactic absorption) to our BBXRT data, we measure the ratio of normalizations of the two components (defined as hard/soft at 1 keV) to be 0.89 ± 0.15, consistent with the ratio 0.79 ± 0.12 observed during the *EXOSAT* era. This confirms the result of TP88 that the two spectral components track each other on long (years) time scales, having varied together by factors of ~ 7, over an 8 yr baseline, and thus that the break to the soft excess has probably been close to 1 keV in all the observations to date.

Examination of the two power-law model shows that the soft component quickly becomes insignificant in the hard X-ray band and provides a negligible contribution to counts above ~ 2 keV. This indicates that the soft excess did not significantly contaminate either the *Ginga* LAC data (nominally covering 2–20 keV) or the *EXOSAT* ME data (covering 1.5–10 keV). In fact, fitting the ME data alone, TP88 obtained $\alpha_{ME} \sim 1.0$, which both the BBXRT data and the *Ginga* data (see next section) suggest is a better representation of the hard component.

No significant iron K emission line is observed in the BBXRT data, with the 1 σ upper limit of 200 eV. No significant iron K edge is observed either, with a 1 σ upper limit of $\tau_{Fe} \lesssim 2$ for an edge in the range 7–8 keV. No significant edge is detected in the soft X-ray regime either.

3.2. *The Ginga Data*

After background subtraction, the 2–20 keV *Ginga* data were tested against the same simple models described in the preceeding section (Table 3). The mean spectral index $\alpha_{2-20} =$

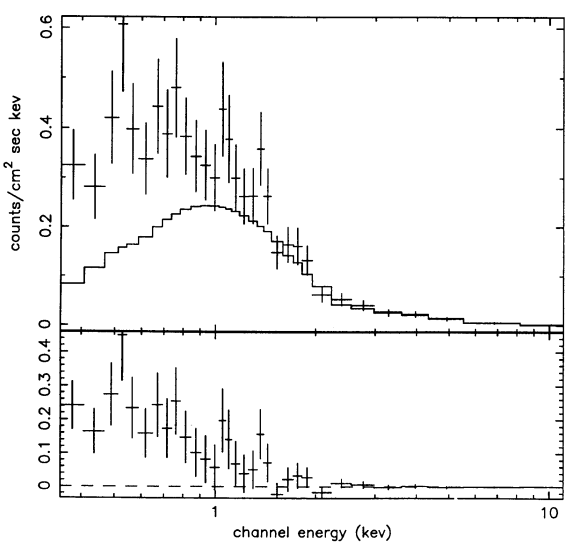

FIG. 1*a*

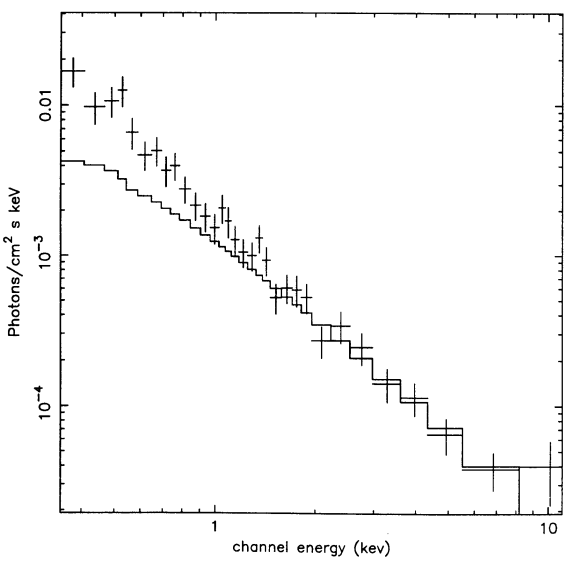

FIG. 1*b*

FIG. 1.—BBXRT spectrum of Mrk 335. Shown are (*a*) the counts spectrum and model fitting residuals and (*b*) the photon spectrum. In both cases the solid line shows the best-fit 2–10 keV power-law spectrum, absorbed by our galaxy, extrapolated below 2 keV.

TABLE 3

POWER-LAW FITS TO THE *Ginga* DATA

Observation	Energy Range	A_{pl} ($\times 10^{-3}$)	α	N_H (10^{21} cm^{-2})	χ_r^2/d.o.f.
1987.....	2–20	4.0	0.99 ± 0.20	14^{+9}_{-5}	0.89/28
1988.....	2–20	9.7	1.11 ± 0.07	$0.0^{+1.5}_{-0.0}$	0.37/28
1987.....	5–20	2	1.31 ± 0.31	...	0.61/23
1988.....	5–20	9.7	1.09 ± 0.14	...	0.37/23

NOTES.—Error ranges are 90% confidence for one parameter of interest ($\chi^2 + 2.7$). A_{pl} is the normalization at 1 keV in photons cm^{-2} s^{-1}.

1.10 ± 0.06 confirms an unusually steep power law for this Seyfert as compared to other AGN.

To confirm that the soft component, observed in the BBXRT data does not provide significant counts in the *Ginga* data, we fitted the data above 5 keV and compared the spectral index to that obtained from the broad-band fit. The derived mean 5–20 keV index is consistent with the power law index found in the broader energy band ($\alpha_{5-20} \sim 1.20 \pm 0.11$), implying that the hard X-ray slope of Mrk 335 is in fact intrinsically steep and that the steepness is not due to any confusion with the known soft excess.

The power-law index of ~ 1.1 is steeper than the "canonical" 2–10 keV index of ~ 0.7 found in many Seyfert galaxies (e.g., Mushotzky 1984; Halpern 1982; Turner & Pounds 1989; Turner et al. 1991). Sensitive observations above 10 keV with *Ginga* revealed a spectral flattening above ~ 10 keV in many similar Seyferts, interpreted by Pounds et al. (1990) as evidence for Compton reflection from cold, optically thick material (e.g., Lightman & White 1988). In this composite scenario, the sum of the steep intrinsic component of $\alpha \sim 0.9$ plus the flat Compton hump appear as a single power-law index of $\alpha \sim 0.7$. The rather steep *Ginga* index in this simple power-law parameterization argues for an absence of the reflection component in the data available to date. We will return to this point in the discussion.

No strong evidence for Fe Kα line emission was found in these spectra. Formally we find values of the F-statistic of 3.0 and 4.1, respectively, for inclusion of a narrow Gaussian line to the model for the 1987 and 1988 observations, the latter being a detection at the ($\sim 90\%$) confidence level. However, examination of the data-model residuals suggests that the observed excess at ~ 6.5 keV amounts to no more than ~ 0.04 counts s^{-1}, of the same order as the systematic error arising from the background subtraction, thus reducing the significance of the emission line in these data. The derived upper limits to the equivalent width of an iron Kα emission line are less than 500 eV (as noted above) and less than 240 eV for the 1987 and 1988 data, respectively, comparable to the limits from BBXRT data. This is consistent with the observed mean for Seyfert galaxies for the *Ginga* sample as a whole (~ 140 eV).

The main difference between the two *Ginga* data sets is in the derived column density. While the 1988 observation shows no evidence for a column greater than a few $\times 10^{21}$ cm^{-2}, to which *Ginga* is sensitive, the 1987 observation requires a much larger column density $\sim 1.4 \times 10^{22}$ cm^{-2}. To further quantify this spectral variability, the PHA spectra from the two observations have been divided by each other. The resultant spectrum is shown in Figure 2, and clearly indicates that the bulk of the spectral change occurs below ~ 5 keV.

We consider three possible origins for the spectral variability:

1. Intrinsic spectral index variations;

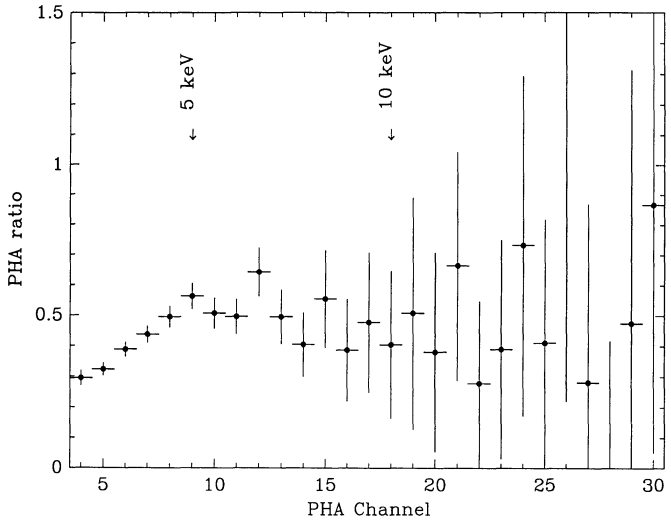

FIG. 2.—Ratio of the 1987 to 1988 *Ginga* spectra, where the 1988 data are the denominator. The ratio indicates the spectral difference between the two, which we interpret as a variation in absorption.

2. A variable soft component (relative to the hard component);
3. Variable absorption.

The first of these can be ruled out at greater than 90% confidence, as a power-law fit to the 1987 observation with N_H fixed at the Galactic 21 cm value gives an unacceptable statistic ($\chi_r^2 = 1.35/25$ d.o.f.; cf. Table 3, row 1), whilst allowing N_H to be free improves the fit with $F = 12.9$, significant at a greater than 99% level. Historically, there is no evidence of a variable energy index for this source. This is illustrated by Figure 3, which shows the ~ 2–10 keV spectral indices from *HEAO* A-2, *Einstein* Observatory MPC (Lee et al. 1988), *EXOSAT* (TP88), and *Ginga* and BBXRT (this work) plotted against flux. The spectral indices are entirely compatible with a constant $\alpha_{mean} = 1.08 \pm 0.03$ ($\chi_r^2 = 0.33/12$ d.o.f.).

A variable soft component, as that observed in our BBXRT data, seems unlikely to be the cause of the observed spectral variability between the *Ginga* data sets. That is because the soft

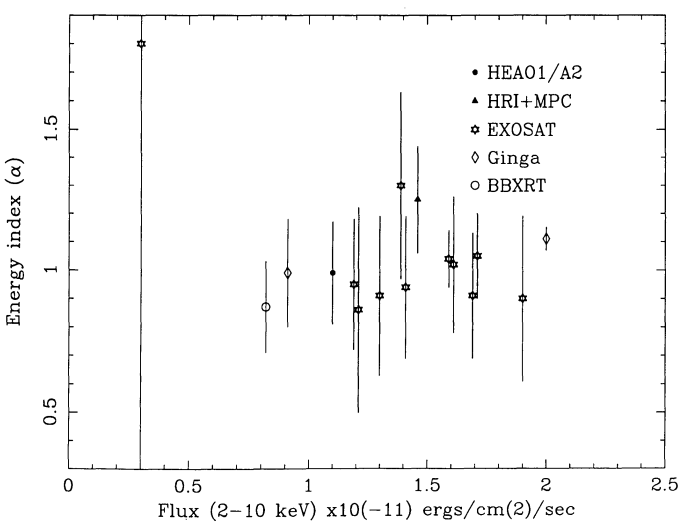

FIG. 3.—Power-law spectral indices derived from the archival and current data (*HEAO* A-2, *Einstein* Observatory MPC, *EXOSAT*, *Ginga*, and BBXRT values are plotted).

component is too steep to provide significant counts in the LAC data, as discussed above.

We conclude that the third mechanism, a variable absorption column, is the most likely explanation of the observed spectral changes. A crucial point to note here is that a significant improvement in χ^2 is evident when an absorption edge is added to the model for the 1987 spectrum. In this case we find $F = 7$, with edge energy $E_{\rm th} = 7.4^{+1.4}_{-0.7}$ keV and depth $\tau_{\rm Fe} = 0.95^{+1.1}_{-0.7}$, corresponding to equivalent hydrogen column density (at Solar abundances) $N_{\rm HFe} = 7^{+9}_{-6} \times 10^{23}$ cm^{-2}. A comparable absorption can be ruled out of the BBXRT data at greater than 99% confidence, where the source is at a similar flux state, and so the variable absorption is not directly correlated with flux.

The inconsistency between the opacity at the iron edge and at soft X-ray energies in the 1987 *Ginga* data could have one of two origins, either an overabundance of iron in the absorber, or partial ionization of the absorber such that elements lighter than Fe are stripped. The degree of inconsistency between the two opacities would require a factor $\sim$10–100 overabundance of iron in this source, which seems somewhat contrived. Also, with a roughly spherical distribution of absorbing material, a $\sim$800 eV Fe Kα line is predicted for such a large column (Inoue 1989), while the 68% confidence limit on the Fe line is 500 eV in the 1987 *Ginga* data. If we increase the Fe abundance in this material, then the predicted Fe Kα line would increase, resulting in an inconsistency with the observed Fe line limit.

An ionized absorber may provide a more plausible alternative. Although the edge energy is formally compatible with the 7.1 keV expected for cold iron, the best-fit value is suggestive of partially ionized line-of-sight material (see, e.g., Turner et al. 1992), in common with $\sim$50% of sources observed with *Ginga* (Nandra 1991). This edge energy suggests that the material has an ionization state such that significant opacity is observed *below* the Fe K edge, which could account for the large soft X-ray column density required for this observation. A fit has therefore been made to the 1987 *Ginga* observation with a partially ionized absorber. We employ the photoionization code described by Yaqoob & Warwick (1991) and assume a two power-law ionizing spectrum, with a soft component of the form suggested by the BBXRT data, and the harder power-law left free. This gives an ionization parameter $U = 20(2\text{–}45)$, corresponding to $\xi \approx 200$ and a column density of $5.5(>0.8) \times 10^{23}$ cm^{-2} (ξ is defined as L_x/nD^2, where L_x is the luminosity over 13.6 eV to 13.6 keV band, $n = 3 \times 10^9$ cm^{-3} is the atom density, D is the distance from the photoionizing source. The temperature has been fixed at 10^5 K). However, in this fit we find a very steep slope ($\alpha \sim 1.6$) for the hard power law. Fixing the slope at the mean value of $\alpha = 1.08$, which may be more realistic, gives $U = 2.2(0.2\text{–}30)$ or $\xi \sim 20$ and $N_{\rm H} = 80(20\text{–}400)$. Inclusion of U as a free parameter gave $F = 5.3$, an improvement at greater than 90% confidence. No edge is required in the 1988 data, with an upper limit of $\tau_{\rm Fe} < 0.42$, corresponding to $N_{\rm HFe} < 3 \times 10^{23}$ cm^{-2} at 7.4 keV. We note that up to $\sim$Fe XVIII the fluorescence yield (and hence the predicted Fe Kα line strength) does not increase appreciably (cf. Krolik & Kallman 1987; Turner et al. 1992).

4. THE ARCHIVAL DATA

Refitting the archival *HEAO 1*/A-2 data yields a 2–10 keV energy index of 0.99 ± 0.18 for a 2–10 keV flux level of 1.1×10^{-11} ergs cm^{-2} s^{-1}, confirming our hypothesis that this source has never shown any evidence for a flat hard X-ray spectrum (Fig. 3). These data also allow us to exclude an iron edge between 7.1 and 7.7 keV at the level of $\tau_{\rm Fe} \lesssim 0.80$ (at 68% confidence for $n - 1$ interesting parameters). At the same level of confidence, the upper limits on an iron line fitted at 6.4 and 6.7 keV are 320 and 360 eV, respectively.

The published *Einstein* HRI + MPC data document an energy index of $\alpha = 1.25 \pm 0.19$ for a flux level of 1.46×10^{-11} ergs cm^{-2} s^{-1} (Lee et al. 1988). These data also confirm the variability in the soft excess component in Mrk 335, reporting an X-ray variation with a doubling time of $\lesssim 10^4$ s, with the variability being most pronounced at the softest X-ray energies (also reported in the *EXOSAT* observations of TP88) and the spectrum being softer after the observed "flare" than before it.

Fitting three of the best signal-to-noise *EXOSAT* spectra (1985 July 21, November 30, and December 24) we obtained a marginally significant detection of an 8 keV edge in the 1985 July data with $\tau = 2.1$ ($N_{\rm HFe} = 1.6 \times 10^{24}$ cm^{-2}) for a 2–10 keV flux of 1.2×10^{-11} ergs cm^{-2} s^{-1}. No significant edge was detected for the November 30 or December 24 observations, which had flux states of 1.64 and 1.60×10^{-11} ergs cm^{-2} s^{-1}, respectively. The December observation gave an upper limit of $\tau \approx 2$ ($N_{\rm HFe} \approx 1.6 \times 10^{24}$ cm^{-2} for a $\sim$8 keV edge).

5. DISCUSSION

5.1. *The Nuclear Source*

The continuum spectrum of the source can be explained as arising in the nucleus via the $e^{\pm}$ pair model (e.g., Guilbert, Fabian, & Rees 1983) for which a schematic diagram is shown in Figure 4 (Svensson 1987, 1992; Lightman & Zdziarski 1987; Zdziarski et al. 1990b, hereafter Z90; Zdziarski & Coppi 1991, hereafter ZC91). In that model, pairs, presumably accelerated

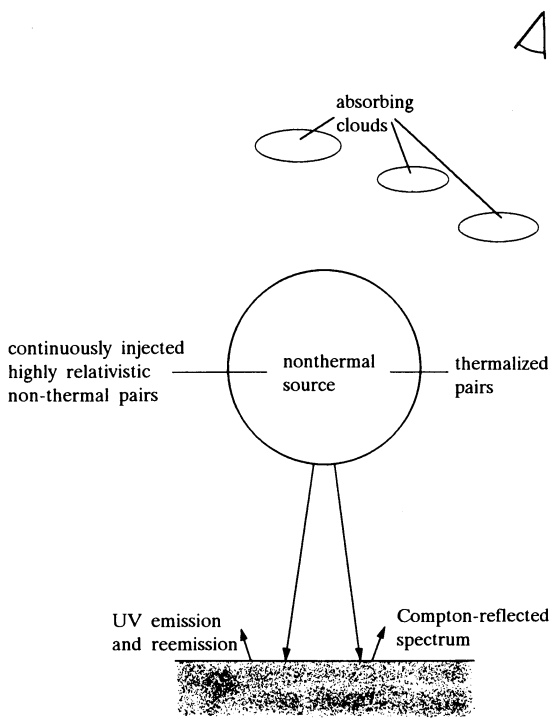

FIG. 4.—Schematic representation of the nonthermal pair model used to interpret the data. See the text for details.

by shocks, magnetic field reconnection, or another mechanism, are injected at relativistic energies into a compact region. The resulting pair cascade gives rise to a hard X-ray spectrum with $\alpha \simeq 1$ through Compton upscattering of UV photons, provided that the ratio of the source luminosity to source size is sufficiently large, and the radiation energy density is larger than the magnetic energy density. The pairs of the cascade decelerate and thermalize, forming an optically thick thermal component within the nonthermal source. The thermalized pairs again Compton upscatter UV photons with the resultant spectral index being a function of the pair temperature and optical depth. From energy balance, the soft X-ray spectral index is greater than 1, and can vary independently of the variations in the amplitude of the hard power law (ZC91). We interpret the soft excess observed in the BBXRT data as due to the upscattering of the UV photons by the thermalized pairs. In the model, the UV photons originate in cold material such as an accretion disk or clouds. Compton reflection occurs when the hard X-rays produced by pair upscattering are incident on this cold material (e.g. Guilbert & Rees 1988; Lightman & White 1988).

The main parameter of nonthermal pair models is the hard compactness, l_h, corresponding to the power, L_h, supplied to the relativistic electrons and reradiated as hard radiation within the nonthermal source of the characteristic size, R,

$$l_h \equiv \frac{L_h \sigma_T}{R m_e c^3} \gtrsim \frac{L_h(1 + \tau_T/3)/\Delta t}{10^{39}\ \mathrm{ergs\ s^{-2}}}\,, \tag{1}$$

where σ_T is the Thomson cross section and m_e is the electron rest mass. The approximate inequality (cf. eqs. [2c]–[2e] in Lightman & Zdziarski 1987) follows from the light travel argument and diffusion in an optically thick source, where Δt is the doubling time scale of the hard component and τ_T is the Thomson optical depth of thermalized electrons in the nonthermal source. An important point is that the emergent spectral shape of the primary continuum is sensitively dependent on l_h. Thus, for a given source there are two independent methods of estimating the hard compactness: from fitting of data to the pair-cascade model spectral forms (see Table 4 below), and from the ratio of the hard luminosity to the characteristic doubling time scale (see eq. [2] below).

The second most important parameter of the model is the soft compactness, l_s, which is defined analogously to l_h (eq. [1]), but with L_h replaced by the *fraction* of the UV luminosity incident on the nonthermal source. The strength of the soft X-ray excess depends strongly on l_s/l_h (see ZC91). The remaining parameters are: the Lorentz factor γ_i at which relativistic pairs are injected, the temperature T_s of the UV photons, and the relative normalization of the reflection contribution r, defined as the ratio of the nonthermal source flux directed towards the cold matter to the flux directed outward. ($r = 1$ corresponds to the isotropically-emitting source located above an infinite slab of cold material.)

The model parameter space is constrained by several considerations. A lower limit on l_h can be obtained from time variability data. Taking the *EXOSAT* hard X-ray doubling time scale of ~ 3000 s (TP88) at a 2–10 keV flux state of 8.4×10^{-12} ergs s^{-1} (as measured by BBXRT), corresponding to the 2–10 keV luminosity of $\sim 2.5 \times 10^{43}\ h^{-2}$ ergs s^{-1}, we estimate (see eq. [1])

$$l_h \gtrsim 80h^{-2}(1 + \tau_T/3) \simeq 80h^{-2}[v + (v-1)^{1/2}] \simeq \begin{cases} 200\,, & h = 1\,; \\ 30\,, & h = 2\,, \end{cases} \tag{2}$$

where $h \equiv H_0/50$ km s^{-1} Mpc^{-1}, $L_h \sim 10 L_{2-10\,\mathrm{keV}}$, which is typically the case for pair model spectra $\tau_T/3 \simeq l_h^{1/2}/10$ from the pair theory (Svensson 1987; Lightman & Zdziarski 1987), and $v \equiv 1 + 0.4\ h^{-2}$. The large value of compactness parameter in Mrk 335 and the implied likelihood of the presence of $e^{\pm}$ pairs in this object was originally pointed out by Lee et al. (1988).

On the other hand, the sum of the compactnesses in the hard (direct and reflected) and soft photons is related to the ratio of the bolometric luminosity in units of the Eddington luminosity, L/L_E, and the source size in units of the minimum stable orbit, $R/3R_g$ (Svensson 1992), which gives

$$l_s + l_h(1 + 0.15r) \lesssim 2 \times 10^3 \left(\frac{L}{L_E}\right)\left(\frac{3R_g}{R}\right), \tag{3a}$$

where 0.15 is the approximate value of the integrated albedo for pair model spectra (Z90), and the presence of the nonthermal source on both sides of the disk was assumed. We will assume here $L \leq L_E$, $R \geq 3R_g$. Hence,

$$l_s + l_h(1 + 0.15r) \lesssim 2 \times 10^3\,. \tag{3b}$$

The value of T_s is determined by the other model parameters and geometry. We assume here that the cross section of the nonthermal source equals πR^2. The UV flux incident on the source is assumed to be diluted blackbody, with the dilution factor $f \leq 1$. Then the corresponding blackbody temperature is given by

$$kT_s \simeq 35 h^{1/2} f^{-1/4} \left(\frac{l_s}{l_h}\right)^{1/4} \left(\frac{l_h}{10^3}\right)^{1/2} \mathrm{eV} \simeq 30\ \mathrm{eV}\,, \tag{4}$$

where 30 eV is an approximately self-consistent value of kT_s, i.e., one corresponding to the obtained values of l_h and l_s (see below) and for $h = 1$ and $f = 1$. The latter equality corresponds to the nonthermal source close to the cold matter, which is consistent with the result of the fit of $l_s/l_h \gtrsim 1$, see below. We kept kT_s fixed at 30 eV in the presented fits.

The injection Lorentz factor is limited to,

$$10 \lesssim \gamma_i \lesssim 1400\,, \tag{5}$$

where the lower limit is due to the model assumption that the injected pairs are highly relativistic and the upper limit is given by the assumption of the Thomson limit for Compton scattering, $4\gamma_i(3kT_s/m_e c^2) \lesssim 1$. The allowed reflection enhancement factor r, is constrained by the upper limits on the equivalent width of the Kα line (§ 3.2). The limits of 500, 240, and 200 eV for the 1987, 1988, and 1990 data, respectively, correspond to

$$0 \leq r \leq 5.6\ (1987)\,,\quad 0 \leq r \leq 2.7\ (1988)\,,\quad 0 \leq r \leq 2.2\ (1990)\,, \tag{6}$$

where we used the value of the equivalent width of 90 eV corresponding to $\alpha = 1.1$ and semi-isotropically illuminated slab (i.e., with $r = 1$) obtained by George & Fabian (1991). Our obtained upper limits are below the theoretically estimated maximum values due to anisotropy of relativistic Compton scattering and geometry (Fabian et al. 1990; Ghisellini et al. 1990; Rogers 1991).

The source size follows from equation (1),

$$R \simeq \frac{7 \times 10^{15} h^{-2}}{l_h}\ \mathrm{cm}\,, \tag{7}$$

where we used the same estimate of L_h as in equation (2). We note that the model is very weakly dependent on R, through the Coulomb and bremsstrahlung rates. In our fits, the size was

TABLE 4

FITS OF THE PAIR MODEL

Observation	Energy Range	l_h	l_s/l_h	r	N_H (10^{21} cm^{-2})	χ^2_r/d.o.f.
1987.....	2–20	880^{+90}_{-350} [a]	$0.27^{+0.59}_{-0.16}$ [a]	$5.6^{+0}_{-5.4}$ [b]	$7.6^{+11}_{-7.6}$	0.65/26
1988.....	2–20	760^{+20}_{-170} [a]	$1.1^{+0.1}_{-0.4}$ [a]	$2.7^{+0}_{-1.3}$ [b]	0.4(f)	0.43/27
1990.....	0.4–10	350^{+340}_{-280} [a]	$1.4^{+1.3}_{-0.8}$	$0.7^{+1.5}_{-0.7}$ [b]	0.4(f)	0.64/28

NOTES.—Error ranges are 90% confidence limits for one parameter of interest; $\gamma_i = 10^3$, $kT_s = 30$ eV, $R = 10^{13}$ cm.

[a] Parameter range given by eq. (3b).

[b] Parameter range given by eq. (6).

kept fixed at an approximately self-consistent value of $R = 10^{13}$ cm (which is also consistent with the time variability data, cf. eq. [2]).

The pair-cascade model has been incorporated into the standard X-ray spectral fitting package XSPEC (Schafer, Haberl, & Arnaud 1991). The pair model used is described in Lightman & Zdziarski (1987), with modifications given in Zdziarski, Coppi, & Lamb (1990a). The reflected component is calculated as in Z90. We independently fitted the BBXRT and *Ginga* spectral data to the pair-cascade model with cold absorption. We give the fit parameters and the underlying assumptions in Table 4. Figure 5 shows the intrinsic spectrum of the nuclear region for the best-fit model of the 1987 *Ginga* observations.

We see that, remarkably enough, both *Ginga* and BBXRT results are best-fitted by similar parameters, i.e., $l_h \sim 10^3$, $l_s \sim l_h$. The high values of l_h and l_s suggest that the AGN luminosity is close to L_E and the nonthermal source size is close to $3R_g$ (eq. [3a]). The large values of l_h result from the steep X-ray spectrum of the object ($\alpha \gtrsim 1$). This is because $\alpha = 1$ in the pair models is obtained in the limit of many pair generations, which occurs at $l_h \gg 10^2$ (Svensson 1987). Note that if instead of monoenergetic injection of primary relativistic electrons a power law injection is used, large l_h would no longer be required (Lightman & Zdziarski 1987).

The allowed parameter region obtained is found to be significantly constrained by inequality (3b). In Table 4, the confidence regions that are reduced by equation (3b) are denoted by "a." We have also found that good fits can be obtained for almost any γ_i in the range given by equation (5). This is due large l_h, at which the self-consistent spectrum is strongly pair-reprocessed and weakly depend on γ_i and T_s. We kept γ_i fixed at 10^3, close to the boundary of the Thomson limit, which value is expected from considerations of pair cascades (Zdziarski 1988).

The large value of the compactness parameter suggested for Mrk 335 by the pair model implies that this steep observed spectrum will break to an even steeper spectrum above ~ 10 keV. The reason for this is that the fractional energy loss in a Thomson downscattering is proportional to the photon energy, which in turn causes a continuum spectrum to break at an energy $\sim m_e c^2/\tau_T^2 \sim 10 m_e c^2/l_h$ (see, e.g., Svensson 1987, 1992; ZC91). The fact that we observe no change in power-law spectral index across the *Ginga* bandpass suggests that we should reconsider our earlier conclusion that no Compton

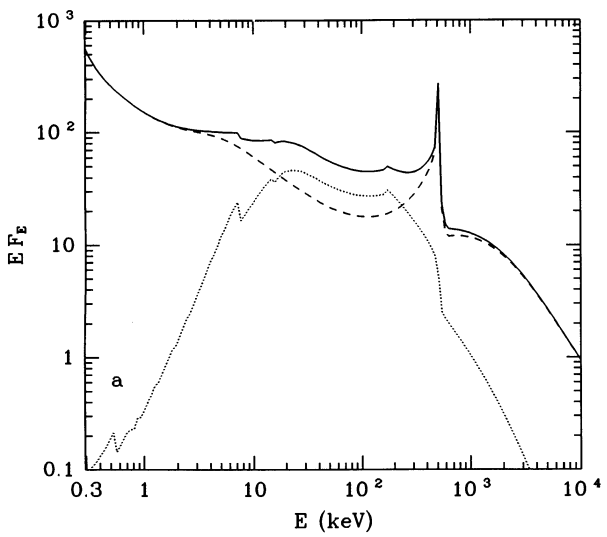

FIG. 5a

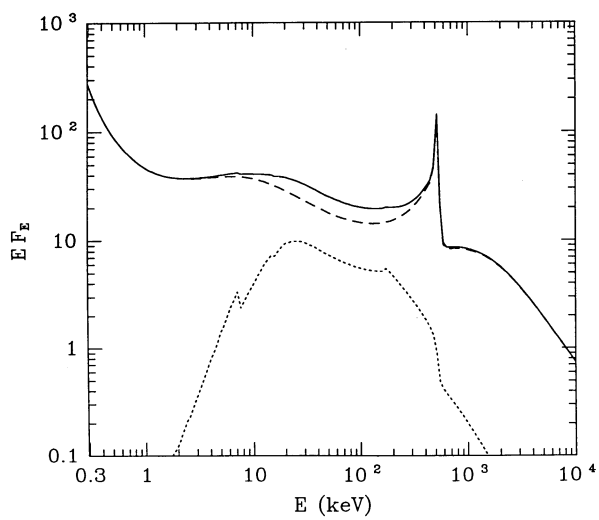

FIG. 5b

FIG. 5.—Intrinsic broad-band spectrum (*solid curve*) in the pair model corresponding to the best fit to the 1988 *Ginga* data (*a*) and 1990 BBXRT data (*b*) (see § 5.1 for the fit parameters). The plotted quantity is EF_E, which shows where most of the power is radiated. In hard X-rays, the composite spectrum (*solid curve*) is much flatter than the pure pair spectrum (*dotted curve*) due to the strong contribution from the reflection component (*dashed curve*). In soft X-rays, one sees the strong excess above the extrapolation of the hard average power law. The model predicts a break in the spectrum at a few tens of keV, and a thermal annihilation line near 511 keV. The spectrum above the line is strongly pair-absorbed. The kink at 15 keV is numerical, and occurs due to the transition between the two Green's functions described in Lightman & White (1988). The Fe Kα line is not shown.

reflection is present in the spectra. The superposition of the Compton reflection spectrum and a steepening power law results in a spectrum (shown in Fig. 5) which, given the modest energy resolution of *Ginga*, can be well approximated as a single power law. The amount of reflection allowed predicts a reflection-component edge of $\tau_{Fe} \lesssim 0.1$. The optical depth of the edge detected in the 1987 *Ginga* data is significantly greater than this value, and so the requirement for a partially ionized absorber in this source remains. We cannot constrain the reflection component in the BBXRT data due to the bandpass. On the other hand the 1988 *Ginga* data require $r \gtrsim 1.5$ (Table 4). There is a clear prediction that this two-component picture of the observed *Ginga* X-ray spectrum has for higher energies: *the X-ray spectrum should steepen above* ~ 30 keV. This is illustrated in Figure 5. This steepening should be observable with XTE.

5.2. *The Nature of the Absorber*

The reduced low-energy opacity compared to that observed at the iron edge in the 1987 *Ginga* data shows that the absorbing material must be ionized or overabundant in iron. The large overabundance required to explain the edge depth suggests that ionization may be a more reasonable explanation of this discrepancy. This is further supported by the best-fit iron edge energy. Fitting to a partially ionized (warm) absorber model suggests an ionization state for the material of around Fe XV.

The lack of absorption in the BBXRT and *EXOSAT* data at the same flux level as the *Ginga* 1987 observations suggests that the absorption variability observed in the *Ginga* data is not directly correlated with the continuum flux. If the density of the absorber is sufficiently low, then the recombination rate may be sufficiently slow that an absorption-flux correlation could not be observed in data with the sampling obtained here. To observe no correlation in these data then the recombination time scale must be greater than 1 day, but less than 1 yr. The absorbing material density can be constrained using $n_e \sim 3 \times 10^{11}/t_{\rm recomb}$, where $t_{\rm recomb}$ is the recombination time in seconds, thus $10^5 < n_e < 10^7$ atoms cm^{-3}. Alternatively the partially ionized absorbing material may be patchy, and a variable covering fraction may be responsible for the observed absorption variability.

6. CONCLUSIONS

The X-ray spectrum of Mrk 335 shows significant softening below ~ 1.0 keV. This spectrum is well explained by nonthermal $e^{\pm}$ pair models. Such models indicate a very compact pair region in Mrk 335, consistent with the observed time variability behavior. However, other models for the soft excess emission, such as emission from the inner regions of an accretion disk, are not ruled out.

Mrk 335 shows evidence for an ionized line of sight absorber, which is variable on time scales of less than 1 yr. Since this variability is not flux correlated, it indicates either a low density ($10^5 < n_e < 10^7$ atoms cm^{-3}) of the absorbing material or inhomogeneity in the absorber.

We thank Chris Done and Keith Arnaud for their help with installation of the nonthermal pair model in XSPEC, and Tahir Yaqoob for his help with the ionized absorber. This work was supported in part by NASA grant NAG5-1813, and by the Polish State Committee for Scientific Research grant 221129102. K. N. acknowledges the financial support of the SERC.

REFERENCES

Fabian, A. C., George, I. M., Miyoshi, S., & Rees, M. J. 1990, MNRAS, 242, 14P
Ferland, G., Korista, J., & Peterson, B. M. 1990, ApJ, 363, L21
George, I. M., & Fabian, A. C. 1991, MNRAS, 249, 352
Ghisellini, G., George, I. M., Fabian, A. C., & Done, C. 1990, MNRAS, 248, 14
Guilbert, P. W., Fabian, A. C., & Rees, M. J. 1983, MNRAS, 205, 593
Guilbert, P. W., & Rees, M. J. 1988, MNRAS, 233, 475
Halpern, J. 1982, Ph.D. thesis, Harvard Univ.
Hayashida, K., et al. 1989, PASJ, 41, 373
Inoue, H. 1989, in Proc. 23d ESLAB Symp., ed. J. Hunt & B. Battrick (Paris: ESA), 783
Krolik, J. H., & Kallman, T. R. 1987, ApJ, 320, L5
Lampton, M., Margon, B., & Bowyer, S. 1976, ApJ, 208, 177
Lee, M. G., Balick, B., Halpern, J. P., & Heckman, T. M. 1988, ApJ, 331, 154
Lightman, A. P., & White, T. R. 1988, ApJ, 335, 57
Lightman, A. P., & Zdziarski, A. A. 1987, ApJ, 319, 643
Malkan, M., & Sargent, W. 1982, ApJ, 254, 22
Morrison, R., & McCammon, D. 1983, ApJ, 270, 119
Mushotzky, R. F. 1984, Adv. Space Res., 3, No. 10, 157
Nandra, K. 1991, Ph.D. thesis, Univ. Leicester
Pounds, K. A., Nandra, K., Stewart, G. C., George, I. M., & Fabian, A. C. 1990, Nature, 344, 132
Rogers, R. D. 1991, ApJ, 383, 550
Serlemitsos, P. J., et al. 1992, in Frontiers of X-ray Astronomy, ed. Y. Tanaka & K. Koyama (Tokyo: Universal Academy Press), 221
Shafer, R. A., Harberl, F., & Arnaud, K. A. 1991, XSPEC: An X-ray Spectral Fitting Package (ESA TM-09; Paris: ESA)
Stark, A. A., Gammie, C. F., Wilson, R. W., Bally, J., Linke, R. A., Heiles, C., & Hurwitz, M. 1992, ApJS, 78, 77
Svensson, R. 1987, MNRAS, 227, 403
———. 1992 in X-ray Emission from AGN and the Cosmic X-Ray Background, ed. W. Brinkmann & J. Trümper (Garching: Max Planck Institute, MPE Rep. 235), 103
Tananbaum, H., Peters, G., Forman, W., Giacconi, R., Jones, C., & Avni, Y. 1978, ApJ, 223, 74
Turner, T. J., & the BBXRT Science Team. 1992, in Frontiers of X-ray Astronomy, ed. Y. Tanaka & K. Koyama (Tokyo: Universal Academy Press), 535
Turner, T. J., Done, C., Mushotzky, R. F., Madejski, G. M., & Kunieda, H. 1992, ApJ, 391, 102
Turner, T. J., & Pounds, K. A. 1988, MNRAS, 232, 463 (TP88)
———. 1989, MNRAS, 240, 833
Turner, T. J., Weaver, K. A., Mushotzky, R. F., Holt, S. S., & Madejski, G. M. 1991, ApJ, 381, 85
Van Groningen, E. 1987, A&A, 186, 103
Weaver, K., et al. 1993, in preparation
Williams, G. A., King, A. R., & Brooker, J. 1986, MNRAS, 226, 225
Yaqoob, T., & Warwick, R. S. 1991, MNRAS, 248, 773
Zdziarski, A. A. 1988, ApJ, 335, 786
———. 1992, in Testing the AGN Paradigm, ed. S. S. Holt, S. G. Neff, & C. M. Urry (NY: AIP), 291
Zdziarski, A. A., & Coppi, P. S. 1991, ApJ, 376, 480 (ZC91)
Zdziarski, A. A., Coppi, P. S., & Lamb, D. Q. 1990a, ApJ, 357, 149
Zdziarski, A. A., Ghisellini, G., George, I. M., Svensson, R., Fabian, A. C., & Done, C. 1990b, ApJ, 363, L1 (Z90)